Colloid Polym Sci (2006) 284: 1275–1286
DOI 10.1007/s00396-006-1508-5

ORIGINAL CONTRIBUTION

**Shou-Shing Hsieh**
**Hung-Chun Lin**
**Chih-Yi Lin**

# Electroosmotic flow velocity measurements in a square microchannel

Received: 10 November 2005
Accepted: 11 February 2006
Published online: 19 May 2006


S.-S. Hsieh (✉) · H.-C. Lin · C.-Y. Lin
Department of Mechanical
and Electro-Mechanical Engineering,
National Sun Yat-Sen University,
Kaohsiung, Taiwan,
Republic of China
e-mail: sshsieh@mail.nsysu.edu.tw
Tel.: +886-7-5252000
Fax: +886-7-5254215

**Abstract** Experiments were performed using a microparticle image velocimetry (MPIV) for 2D velocity distributions of electroosmotically driven flows in a 40-mm-long microchannel with a square cross section of 200×200 μm. Electroosmotic flow (EOF) bulk fluid velocity measurements were made in a range of streamwise electric field strengths from 5 to 25 kV/m. A series of seed particle calibration tests can be made in a 200×120×24,000-μm untreated polydimethyl siloxane (PDMS channel incorporating MPIV to determine the electrophoretic mobilities in aqueous buffer solutions of 1× TAE, 1× TBE, 10 mM NaCl, and 10 mM borate. A linear/nonlinear (due to Joule heating) flow rate increase with applied field was obtained and compared with those of previous studies. A parametric study, with extensive measurements, was performed with different electric field strength and buffer solution concentration under a constant zeta potential at wall for each buffer. The characteristics of EOF in square microchannels were thus investigated. Finally, a composite correlation of the relevant parameters was developed in the form of $u* = 5.46\,\varsigma^{*0.739} DN^{-2.132} ME_x^{*0.9996}$ within ±1% accuracy for 99% of the experimental data.

**Keywords** Electroosmotic flow · MPIV measurements · A square channel

## Introduction

Electroosmosis is a basic phenomenon experienced in all electrophoretic separation processes. It is the flow generated by the action of an electric field on a fluid with a net charge, which is created by the zeta potential and confined in the Debye layer. This basic phenomenon in the electrokinetic transport is applied in the design of many microfluidic devices/systems being used today [5, 8]. Applications where such phenomena play an important role are in the cooling of microelectronics, lap-on-a-chip diagnostic devices, and in vivo drug delivery systems. In fact, electrically neutral liquids have a distribution of electrical charges near a surface because of a charged surface. This region is known as the electrical double layer (EDL) which induced the aforementioned electrokinetic flow. In addition, hydrophobic materials have become increasingly attractive for use in micropatterned devices. Thus, the flow characteristics of microfluid involving electrokinetic phenomena and liquid slip are needed for design and operation of microfluidics in microelectromechanical systems (MEMS) devices [13].

Contrary to hydrodynamic flows, where one finds a parabolic distribution of the flow velocities with the maximum velocity at the center of the channel and zero velocity at walls, electroosmotic flow (EOF) is generated close to the wall and therefore produces a nearly uniform (i.e., plug-like profile) velocity distribution across the entire cross section of the channel. In most cases, the Debye length of typical electrolytes used in microfabri-

cated electrokinetic systems is much smaller than the hydraulic diameter of the channels. Typical ratios of channel diameter to Debye length are bigger than $10^4$.

The liquid flow rates induced by electroosmotic potentials are typically small with average velocities of the order of a few millimeters per second. Therefore, high-resolution flow diagnosis is important to the development of novel electrokinetic devices. This is particularly true of efforts that aim to characterize nonideal EOF conditions [3]. In recent years, there have been a lot of papers and reports on the electrokinetic phenomenon and the MPIV. Meinhart et al. [10] presented experimental results for PIV measurements of a pressure-driven microchannel flow with emphasis on microfluidic applications. In the same year, Cummings [2] had used an Ar–ion laser to capture the flow pattern in electroosmotically driven flow. These papers showed that variations in the microchannel surface charge can distort the flow distribution.

As stated earlier, the study of flow field in microchannels is of significant interest to engineering and scientists because of emerging applications in high-tech industries such as heat sinks for cooling microelectronics, design of bioanalytical microfluidic devices, miniaturized flow injection analysis systems [1], and microfuel cell fuel delivery systems [6], where a square or rectangular microchannel is the most popular shape to be used in MEMS devices. The most notable advantage of an EOF is that there seems no moving parts in the entire fluid delivery system.

It is known that the main disadvantage of EOF is its strong dependence on the chemistry of the system, which, in turn, is a consequence of the strong dependence of the zeta potential on the chemical state of the system. Such makes EOF hard to control, and every change in pH, dielectric constant ionic concentration, etc. due to reaction or mixing processes has an immediate effect on the magnitude of the EOF. Using buffers can alleviate this situation to some level. Therefore, there is an essential need to further study the hydrodynamic transport characteristics based on parametric consideration for fully developed EOF in a square microchannel with different buffers.

In this paper, we present the velocity distributions of EOF in microchannels with a square cross section of 200×200 μm. The characteristics of EOF in this square channel with four different buffer solutions are investigated experimentally. Wall velocities and velocity profiles are compared to those of previous studies [3, 11, 12] where an electric field is applied along the axis of the microchannel through microparticle image velocimetry (MPIV) measurements. Functional relationship of electroosmotic velocity with relevant parameters was explored, and a composite correlation was finally developed.

## Electrokinetics theory

Referring to Fig. 1, consider a square microchannel of width $2W$, height $2H$ ($W$=$H$, while for a square), and length $L$; the steady-state velocity field in an electrokinetically driven, fully developed flow field in this microchannel can be found through the following analysis.

Following Arulanandan and Li [1], the 2D dimensionless steady-state equations of motion of the present EOF can be written:

$$\nabla^2 u^* = ME_x^* \sinh(\phi^*) , \tag{1}$$

where $u^*$ is the dimensionless velocity ($=u/U$), $E_x^*$ the dimensionless streamwise electric field ($=E_xL/\varsigma$), $\varphi^*$ the dimensionless electric potential $\phi^* = (ze/k_bT)\phi$, $\varepsilon$ the dielectric constant, and $M = \left(2n_0ze\varsigma D_h^2/\mu UL\right)$ incorporating with dimensionless zeta potential boundary condition at channel wall $\varsigma^* = (ze/k_bT)\varsigma$. The present $U$ was chosen as 1 mm/s.

In addition, the electrokinetic effect on liquid flow is modeled by the general Nernst–Planck equation describing anion and cation distributions, the Poisson–Boltzmann equation determining the electrical potential profile, the continuity equation, and Eq. (1), governing the velocity field. Based on the above theoretical analysis, one may find that the present EOFs are influenced by the following

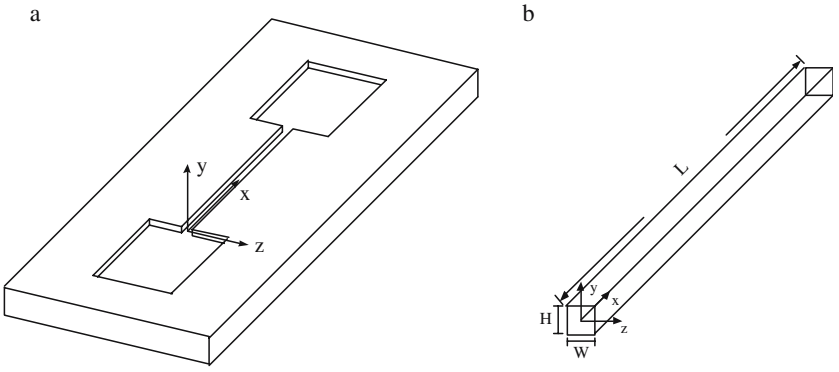


**Fig. 1** Schematic of the test microchannel. **a** 200×120×24,000 μm untreated PDMS channel, and **b** 200×200×40,000 μm borosilicate glass channel

variables and geometric parameters: (a) electric field strength, (b) electrolyte types and concentration, and (c) channel hydraulic diameters [1]. Finally, through dimensional analysis, the present EOF is a function of Debye number (DN), $E_x^*$ and $M$ (in terms of $ME^*$), and $\varsigma^*$. In this study, different electric field strength and four buffers with different ionic strength and a fixed hydraulic diameter in a square microchannel will be experimentally investigated.

## Experimental

### PDMS microchannel fabrication

There were two test structure channels used. One was a 40-mm-long borosilicate glass channel with a square cross section of height 200 μm manufactured by Wilmad Glass for solution particle electrophoretic velocity and wall electroosmotic velocity measurements, and the other was a 200 μm×120 μm×24-mm untreated polydimethyl siloxane (PDMS) channel for particle electrophoretic mobility measurements. The untreated PDMS channels were fabricated in house at the University Microsystem Laboratory by casting a straight open channel from PDMS methyl acrylate and sealed with the same material. The casting mold was made by SU-8 deep UV lithography. Based on the paper of Duffy et al. [4], these channels were used to measure the particle electrophoretic mobility. Detailed SU-8 mold design and PDMS channel fabrication through deep UV lithography can be explained as follows. The fabrication starts with silicon wafers insulation by thermal oxidation. The Su-8 photoresist is spin-coated at 2,000 rpm onto silicon wafers to create masters for 30 s with 120 μm in thickness. A mask is made out of high-solution quartz glass printed to scale to put on the silicon wafers, and then a UV beam (365 nm) is illuminated for a few minutes to make a negative etched channel manifold. During the process, the excess photoresist is peeled off from the silicon substrate that has a negative pattern of the master. Meanwhile, a 10:1 mixture of PDMS prepolymer was poured onto the master and cured for 1 h at 70 °C. After curing, the PDMS replica mold was peeled from the master. Flat pieces of PDMS were formed by casting prepolymer against a silicon wafer and curing. To form enclosed channels, a PDMS replica and a PDMS flat were rinsed in acetone as well as in ethanol and dried with argon stream.

For these two tested channels, precise information of the channel's dimension is extremely important for an accurate evaluation on this EOF channel. The depth, width, and length were measured optically with an accuracy of less than ±0.2%. To understand the present device surface condition, the roughness of the channel was measured along its center with the surface profilometer. The uncertainties for relevant geometric parameters are listed in Table 2.

### Flow system

In the present electroosmotically driven flows, a 40-mm-long borosilicate glass square channel (Wilmad Glass, Buena, NJ, USA) with 200×200 μm cross section is used and has two reservoirs to supply buffer of fluorescent particles for the channel. Before use, the microchannel and the entire flow loop were rinsed with DI water for at least 1 h to remove any contaminants. The transparent nature of the microchannel surfaces allowed visual examination of the channel to ensure that no bubbles were left in the channel. The four buffer solutions used were 1× Tris–acetate with EDTA (TAE), 1× Tris–borate with EDTA (TBE), 10 mM borate, and 10 mM NaCl. A schematic diagram showing the flow channel and the auxiliary system is given in Fig. 2. During the experiments, the above-stated microchannel was connected to two small reservoirs. Current data were recorded from the power source by a personal computer-based data acquisition system. MPIV measurements were taken through a viewing window at the midplane ($y$=0) between the two reservoirs. The potential was applied via platinum electrodes immersed in two 3-ml open reservoirs. The distance between electrodes was 40 mm. The electric field strengths of 2.5, 5, 7.5, 10, 12.5, 15, 17.5, 20, 22.5, and 25 kV/m were applied.

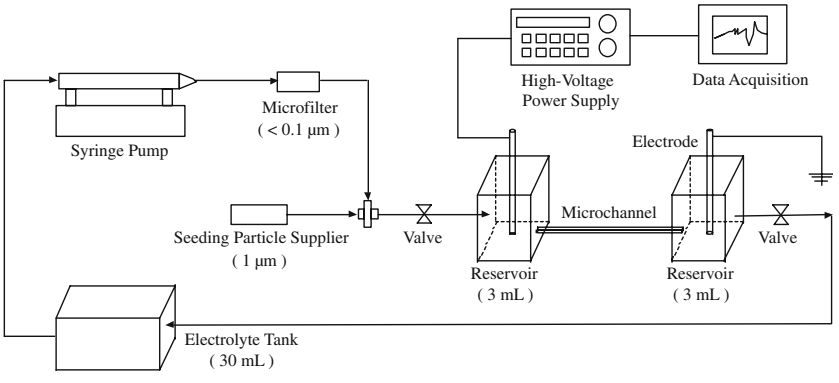


**Fig. 2** Schematic of present experimental flow loop

## MPIV setup

The use of the MPIV technique is very attractive in microfluidics because it helps to understand the detailed flow phenomena in microsystems. The MPIV utilizes flow tracing particles to map the flow in the microchannels. In the study, orange fluorescent particles with 1 μm diameter were used as seeding. The electric field, which was produced by a high voltage, had no effect on the particles. To avoid this effect, it had a high density of carboxylic acids on their surface. These particles had an excitation peak of 535 nm and an emission peak at 575 nm. These particles were surfactant-free. These particles were introduced into the microchannel and electrokinetically driven by a range of electrical fields. Figure 3 is a schematic of the MPIV measurement system used in this study. The system whose layout is reported in Fig. 3 is based on two pulsed Nd:YAG lasers firing on the second harmonic (green 532 nm). The laser pulse duration is 1.5–40 ms based on the velocity magnitude. The test system is mounted on a movable xz stage on an inverted epifluorecent microscope (DMIRM Leica) with 40×, numerical aperture NA=0.55 panchromatic objective and a field view of 400×300 μm. This microscope was equipped with a 12 V, 100 W halogen (Xe/Hg) lamp and a color filter for microscopic imaging. The measurement plane (i.e., object plane) was precisely positioned relative to the test section by moving the objective lens vertically in the y direction and by moving the table horizontally in the x and z directions. As mentioned earlier, orange-fluorescently dyed, 1-μm diameter flow tracing polystyrene particles had an excitation peak of 535 nm and an emission peak at 575 nm. The concentration of fluorescent microspheres based on interrogation volume was $8\times10^7$ particles per milliliter. The images were recorded using a Dantec 80C60 Hisense PIV 1280×1024×12 bit interline transfer camera. A total of five images per second were taken for each flow field with a spatial resolution of 32×32 pixels, and the interrogation cell overlay was 50%. Ensemble averaging of 20 images consecutively captured for 4 s was used to obtain the velocity measurements. The calculated measurement depth of the present MPIV is 5 μm. The present measurements were performed in a clean room of the University Microsystem Laboratory where the ambient temperature was controlled at 298.2 K. Each measurement was repeated at least three times at a specified condition. Noting that the present measurements were conducted at the middle region of the microchannel, the data for inlet as well as exit regions were not available at this stage, and the flow was found to be hydrodynamically fully developed.

## Methodology used (for particle electrophoretic mobility and electroosmotic velocity)

Following Duffy et al. [4], the electrophoretic velocity of the seed particles in the untreated PDMS channel of this study with negligible electroosmotic mobility can be found by using MPIV measurements for this untreated PDMS channel. The total velocity of seed particles was found from MPIV measurements for borosilicate glass channels. After these velocities have been found, the bulk averaged

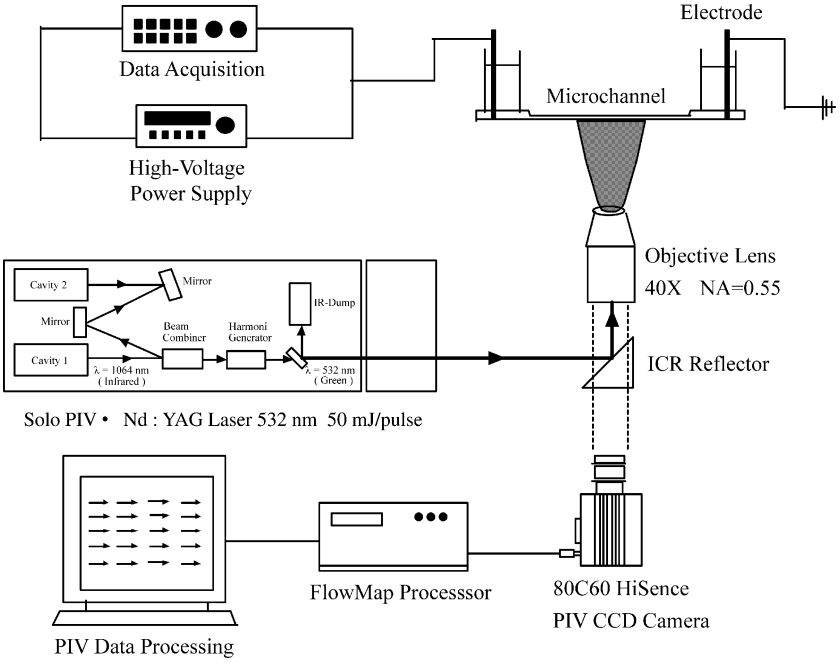


**Fig. 3** Schematic of the MPIV system

velocity of the fluid $u$ for the present EOF is given by the equation:

$$u = \overline{u}_m - \overline{u}_{ph} \ , \tag{2}$$

where $\overline{u}_m$ is the total velocity of seed particles by MPIV in borosilicate glass channels and $\overline{u}_{ph}$ is the electrophoretic velocity of the seed particles in the untreated PDMS channel. With respect to measurement uncertainties, the most significant source of error is expected to be the measurements at the wall.

### Solution preparation

Changes in pH, concentration, dielectric constant, etc. due to reactions and mixing processes make electrometric flow hard to control. To avoid these things to happen, extreme care should be paid in preparing the buffer solutions. The TAE buffer 1× has a pH of 8, while the pH value of the TBE buffer 1× is 8.3. A 10-mM borate buffer solution has a pH value of 9.2, and the pH value of 10 mM NaCl aqueous solution is 7. The 1× TBE was secured from biological industry. The 1× TAE was prepared and contained 40 mM Tris base, 40 mM glacial acetic acid, and 1 mM EDTA in deionized water. Again, like Sinton et al. [12], although both are termed "1×", these buffers differ substantially in ionic strength. In fact, it is difficult to calculate the exact concentration of dissociated ions. This is because the electrokinetic characterizations of these two solutions with various solid surfaces have not been well studied and understood as well. The electrolyte solutions of NaCl and borate buffer were prepared by dissolving NaCl, and NaCl and borate acid (i.e., NaCl+$H_3BO_3$) in deionized water, respectively. The bulk liquid conductivities of the solutions are listed in Table 1. Immediately before use, all solutions were filtered through a 0.1-μm particle filter, and microchannels were rinsed/cleaned with pure water. Then, appropriate buffers were applied. The electrokinetic potential and flow parameter ranges considered in this experimental work are also presented in Table 1.

## Results and discussions

Cross-stream velocity profiles of EOFs in a microchannel with different buffer solutions of a hydraulic diameter $D_h$=200 μm at $E_x$=5, 10, 15, 20, and 25 kV/m are given in Fig. 4a–d. The plug-like motion, a characteristic of EOF, is apparent, and the velocity profiles remain fairly flat right to the wall for each buffer for $E_x \leq 15$ kV/m; while for $E_x$=20 and 25 kV/m, concave-shape velocity profile happens due to Joule heating possibly. Although the local temperature measurements of the buffers were not made, the inlet and outlet temperatures were still measured. The differences seem significant as $E_x$>15 kV/m. A reasonable estimate (as shown later) for the Debye length from the classical theory [7] shows that $\lambda \cong 1$–3 nm for the present four buffers which indicates an EDL thickness on the order of 10 nm. This EDL thickness is much less than the spatial resolutions of the present optical microscopy. Therefore, the velocity profile near the wall may have an artifact. Such situation was also reported by Sinton et al. [12]. Among the four buffers under study, the borate solution has the largest velocity at each applied electric strength $E_x$. Furthermore,

**Table 1** Fundamental physical constants and measurement parameters

| | | | | |
|---|---|---|---|---|
| Fundamental physical constants | | | | |
| Permittivity of vacuum, $\varepsilon_0$ | $8.854187817\times10^{-12}$ F m$^{-1}$ | | | |
| Elementary charge, $e$ | $1.60217733\times10^{-19}$ C | | | |
| Boltzmann constant, $k_b$ | $1.380658\times10^{-23}$ J K$^{-1}$ | | | |
| Command parameters | | | | |
| Electric field, $E_x$ | 2.5, 5, 7.5, 10, 12.5, 15, 17.5, 20, 22.5, 25 kV m$^{-1}$ | | | |
| Absolute temperature, $T$ | 298.15 K | | | |
| Hydraulic diameter, $D_h$ | 200 μm | | | |
| Distance between two electrodes, $L$ | 40,000 μm | | | |
| Reference velocity, $U$ | 1,000 μm s$^{-1}$ | | | |
| Relevant parameters | | | | |
| | 1× TAE | 1× TBE | 10 mM NaCl | 10 mM Borate buffer |
| Dielectric constant, $\varepsilon$ | 77.876 | 77.232 | 78.358 | 78.356 |
| Dynamic viscosity (mPa s), $\mu$ | 0.981 | 1.020 | 0.911 | 0.914 |
| Ionic number concentration ($10^{24}$ m$^{-3}$), $n_0$ | 12.040 | 26.789 | 6.020 | 3.814 |
| Valence of type-I ions, $z$ | 1.000 | 1.000 | 1.000 | 1.000 |
| Debye length (nm), $\lambda$ | 2.143 | 1.431 | 3.040 | 3.819 |
| Electrical conductivity (S m$^{-1}$), $s$ | 0.159 | 0.355 | 0.118 | 0.069 |

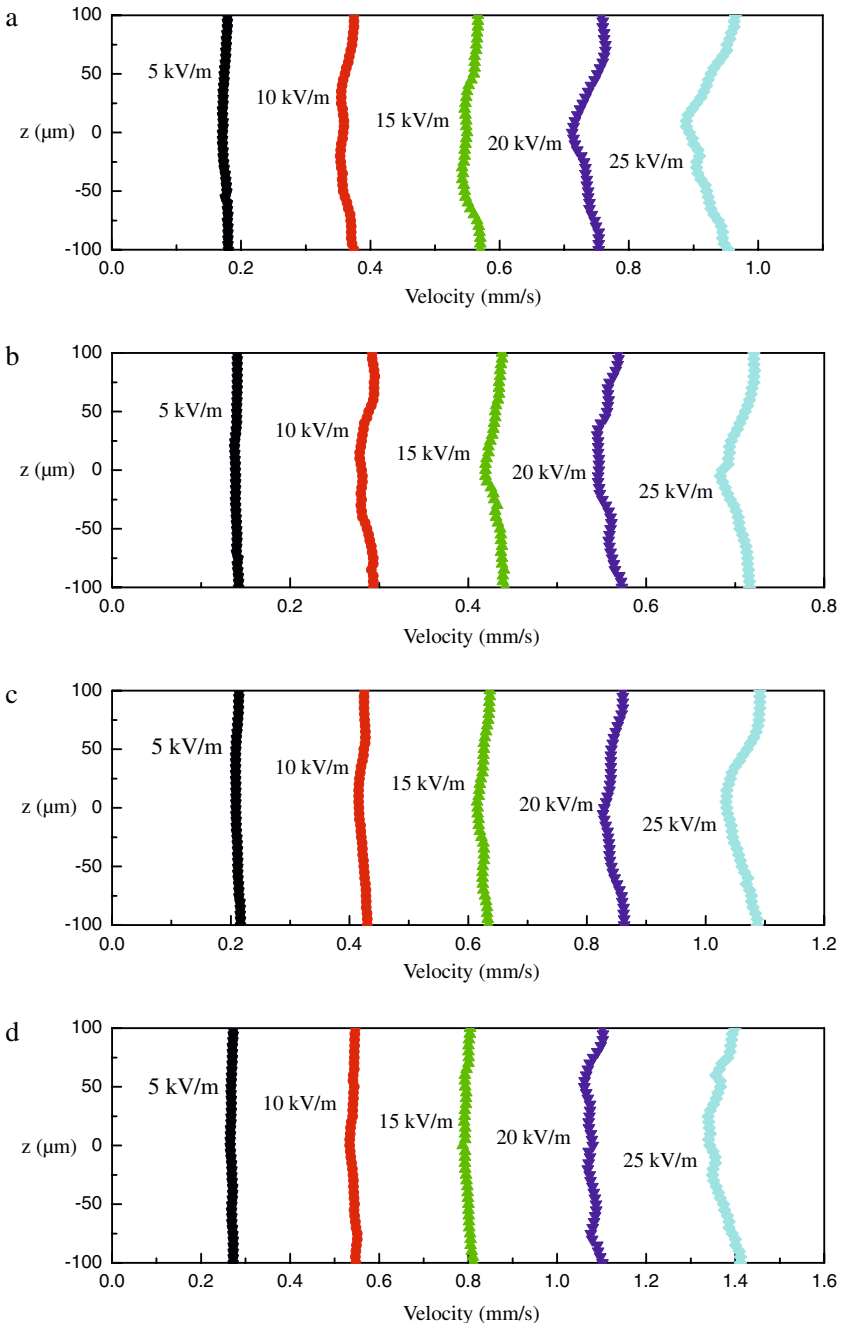


**Fig. 4** Velocity profile from EOF of **a** 1× TAE, **b** 1× TBE, **c** 10 mM NaCl, and **d** 10 mM borate buffer solutions

for $E \leq 10$ kV/m, the velocity profile among four buffers seems very similar; however, at $E=25$ kV/m, a noticeable difference exists. The corresponding vector plots and streamlines ($\psi=0$ at wall) of Fig. 4 at $E_x=5$ kV/m for 1× TAE, 1× TBE, and 10 mM NaCl are shown in Figs. 5a–c. The velocity vectors and the streamlines are consistent. Again, a nearly uniform plug-like flow was observed, and the flow was mostly unidirectional. Because the EOF is driven by body forces concentrated near the surface, the streamlines closely follow the surfaces, and they are parallel to the external electric field which can also be seen in Fig. 5 and are in agreement with those reported from Dutta et al. [5]. An uncertainty estimate for the relevant variables and parameters was made and also listed in Table 2.

Overall, the presence of the concave velocity profile shown in Fig. 4 as $E \geq 15$ kV/m is due to two factors. One is a pressure driving force on the buffer by net charge near the

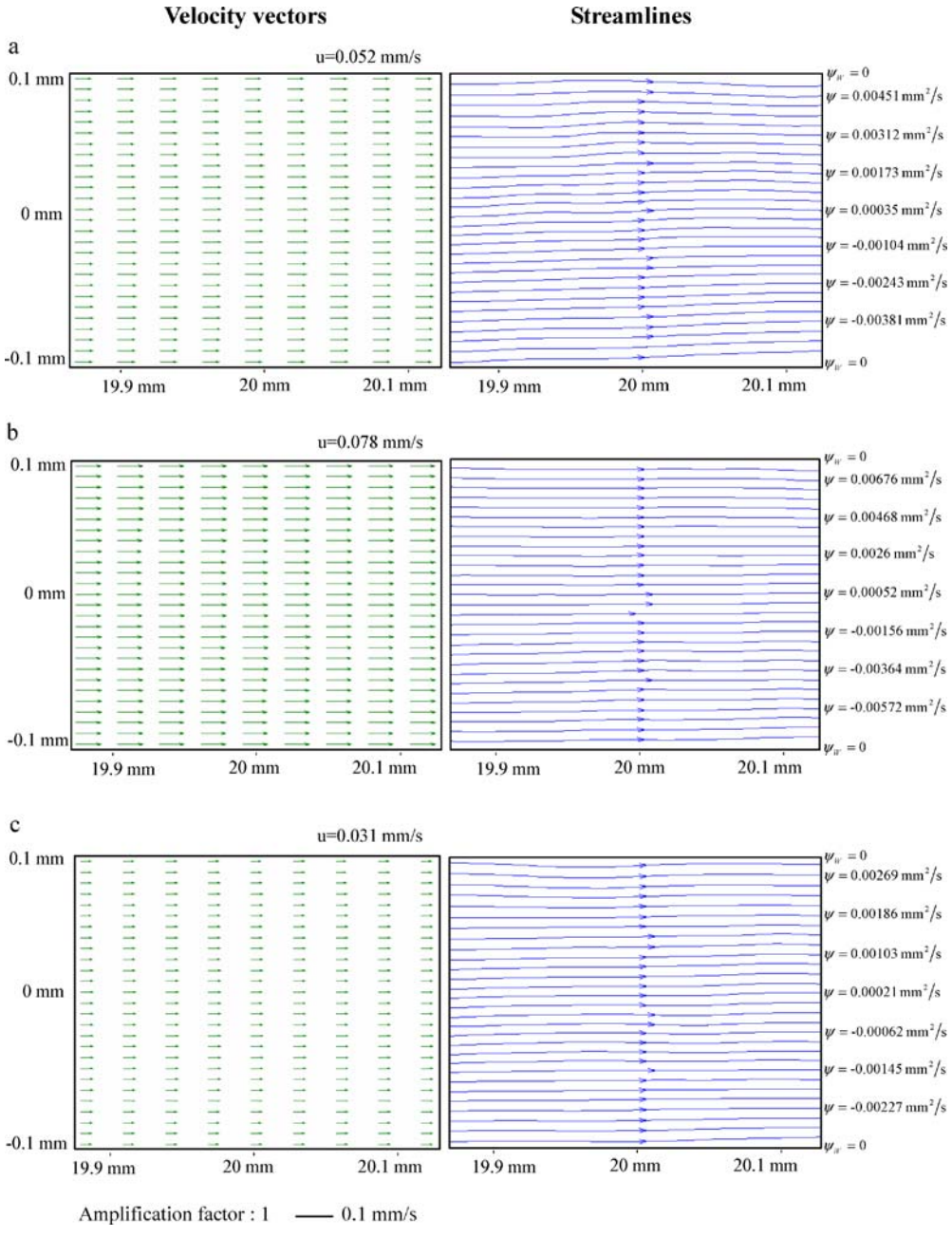


**Fig. 5** Velocity vector distribution and streamline on xz middle plane from electroosmotic and electrophoretic flow of **a** 1× TAE, **b** 1× TBE, and **c** 10 mM NaCl at 5 kV/m

wall, and the other is the viscous drag in the core of the channel. These two factors are counterbalanced. As a result, the flow in the core of the channel has a lower velocity as compared to those flows near the wall. Such situation becomes more noted as the applied electric strength increases. Moreover, the values of the streamlines shown in Fig. 5b again indicate that a plug-like flow covers most part of the channel cross section with a reference value of "zero" set at the channel wall for the present study. One of the typical images of the corresponding flow/particle displacement at a time interval ($\Delta t$) for 1× TAE is shown in Figs. 6a,b for untreated PDMS channel and borosilicate glass channel, respectively. Due to a faster movement of the fluorescent particle in Fig. 6a, the time interval ($\Delta t$) is shorter to be one-fourth of that in Fig. 6b for electrophoretic and EOF measurements. Generally, the movements of electrophoretic particles can be clearly seen in Fig. 6a as compared to those shown in Fig. 6b.

Plots of average electroosmotic velocities vs applied electric field strength for 1× TAE, 1× TBE, 10 mM NaCl, and 10 mM borate solutions based on a constant electrophoretic mobility and those of varied ones are shown in

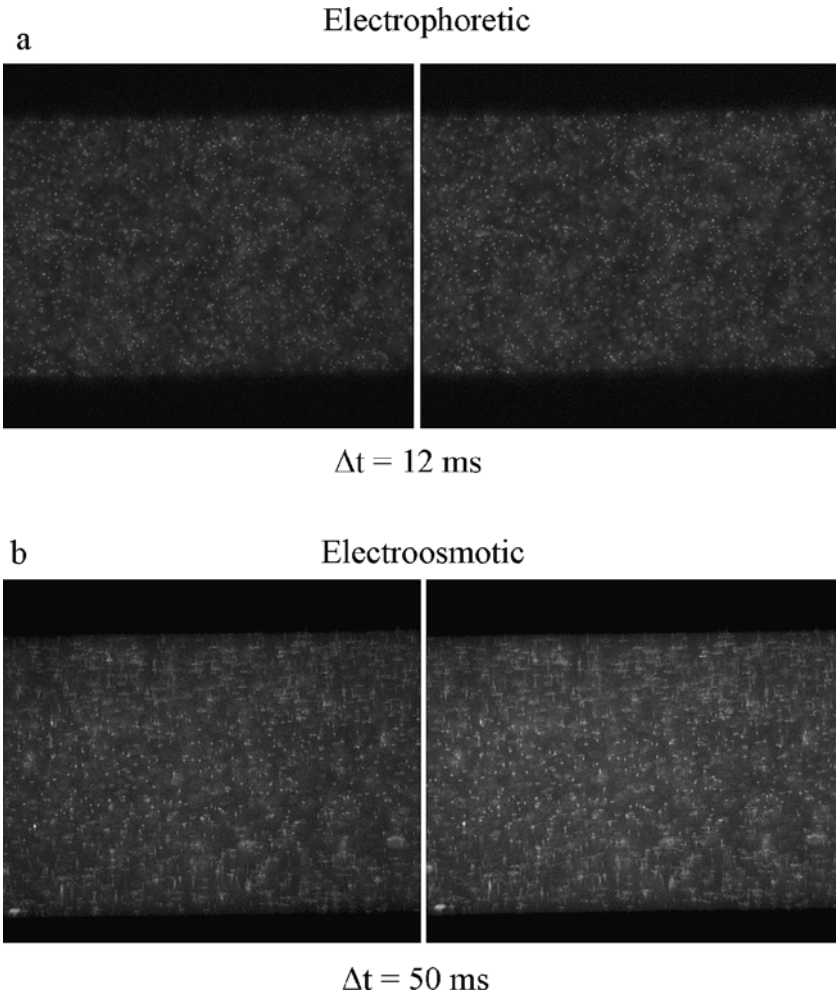


**Fig. 6** MPIV visualization for 1× TAE at 5 kV/m from **a** electrophoretic flow in 200×120×24,000 μm untreated PDMS channel, and **b** electrophoretic and EOF in 200×200×40,000 μm borosilicate glass channel

Fig. 7a,b. A linear increase in velocity with increasing applied field was observed in Fig. 7a for the case of constant electrophoretic mobility. Electroosmotic mobilities of $3.68\times10^{-8}$, $2.84\times10^{-8}$, $4.21\times10^{-8}$, and $5.43\times10^{-8}$ $m^2/V$ s for 1× TAE, 1× TBE, 10 mM NaCl, and 10mM borate solutions, respectively, are listed in Table 3 and compared with those of Sinton et al. [12] for 1× TAE and 1× TBE buffers and with those of Devasenathipathy and Santiago [3] for borate buffer. Nonlinear increase trend is found in Fig. 7b for electrophoretic mobility increase due to Joule heating. This is because the Joule heating makes a variation of the fluid temperature along the microchannel. Taking a close-up view, the lines shown in Fig. 7a with different colors corresponding to different buffers can extend through the origin as expected and have a different slope each. The slope, like the one of Sinton and Li [11], indicates constant electroosmotic and electrophoretic mobilities and that negligible temperature increases due to Joule heating. As stated previously, the measured average electroosmotic and electrophoretic mobilities are also listed in Table 3 for these four buffers, which all exhibited a little bit lower values as compared to those of Devasenathipathy and Santiago [3] and Sinton et al. [12]. On the contrary, the electroosmotic mobility would increase if the Joule heating is considered as the bulk fluid temperature of the buffer rises. This is caused by a counterbalanced effect of viscosity decreasing (increase mobility) and decreasing relative permittivity (slightly decrease mobility) of the medium following Sinton et al. [12]. Consequently, constant electroosmotic and electrophoretic mobilities are not found anymore as shown in Fig. 7b.

Using the Smoluchowski equation [7], the corresponding zeta potentials can be calculated and are also listed in Table 3 where the differences in zeta potentials strongly suggest the different ionic strengths among these four buffers and are compared to those of previous studies [12] for 1× TAE and 1× TBE buffers. Small differences in values are expected. In fact, the zeta potential is strongly dependent on the chemistry, i.e., the chemical composition of the wall material and the chemical composition of the buffer (pH, ionic strength, etc.), as well as the temperature. Again, for four buffers considered herein, the electro-

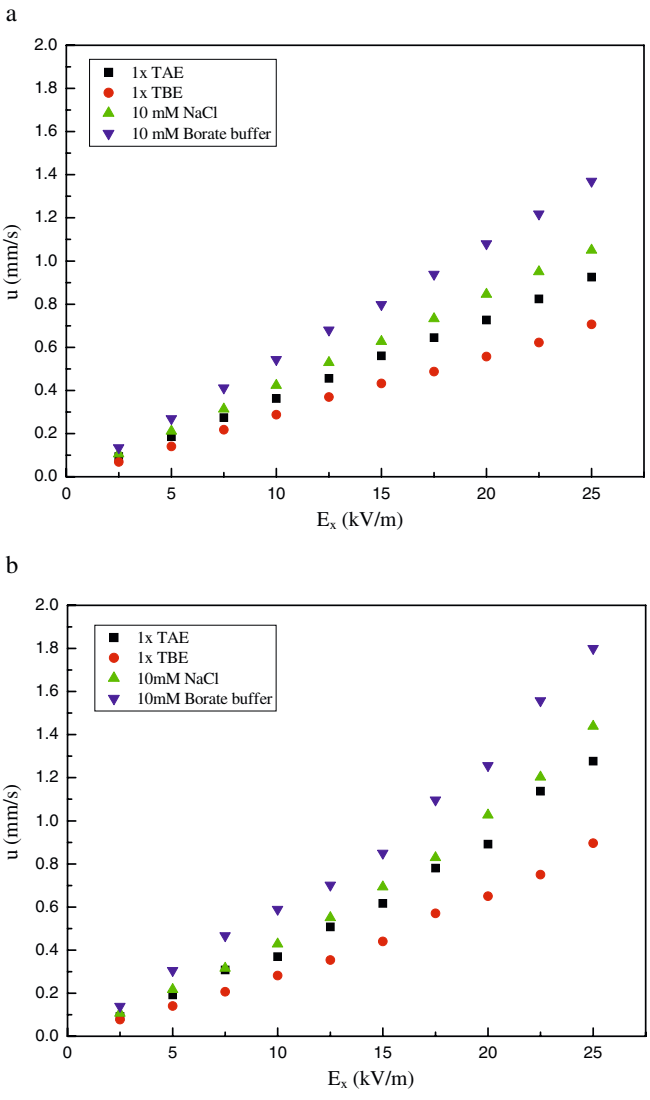


**Fig. 7** Average electroosmotic velocity vs electric field strength **a** without Joule heating, and **b** with Joule heating

osmotic velocity for a relative higher ionic strength in the TBE buffer was the lowest which may not be practical as related to the microfluidic applications. However, the present 10 mM borate buffer has the highest electroosmotic velocity and it can reach to 0.54 mm/s at $E$=10 kV/m. This would provide a competitive potential of applicability in the context of microfluidic technologies as compared to the two commonly used ones in chemical and biological industry like the TAE and TBE buffers. Moreover, it appears that the higher ionic strength would result in the lower electroosmotic velocity for a given buffer solution. This is because the Debye length is very small in concentrated ionic solutions which can also be seen in Table 1. Moreover, the electric conductivity for these four buffers

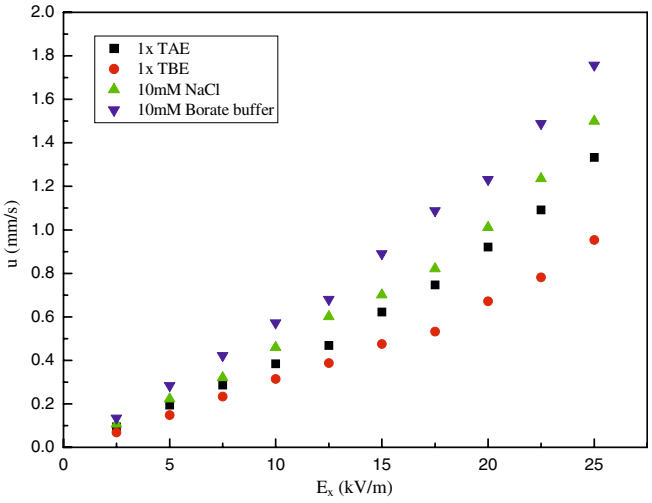


**Fig. 8** Average electroosmotic velocity vs electric field strength by temperature modified method

listed in Table 1 seems to have no significant contribution on Joule heating effect.

With temperature or Joule heating effect considered, the electrophoretic velocity and electroosmotic velocity in Fig. 8 were modified and recalculated following Eq. (3) given by Sinton and Li [11]:

$$u = \frac{\overline{u}_m}{\left(1 - \left(\frac{ze}{6\pi a\varepsilon\varsigma}\right)\right)}, \tag{3}$$

where $\varepsilon$ is the permittivity of the buffer, $\varsigma$ the zeta potential, $z$ the valence, and $a$ the radius of the fluorescent particle,

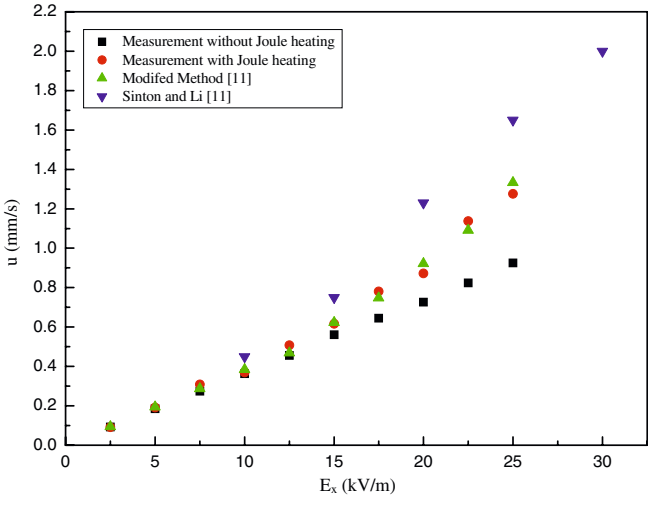


**Fig. 9** Average electroosmotic velocity vs electric field strength for 1× TAE by MPIV measurement results with constant mobility, measurement with Joule heating, the temperature modified method, and the current-based method by Sinton and Li [11]

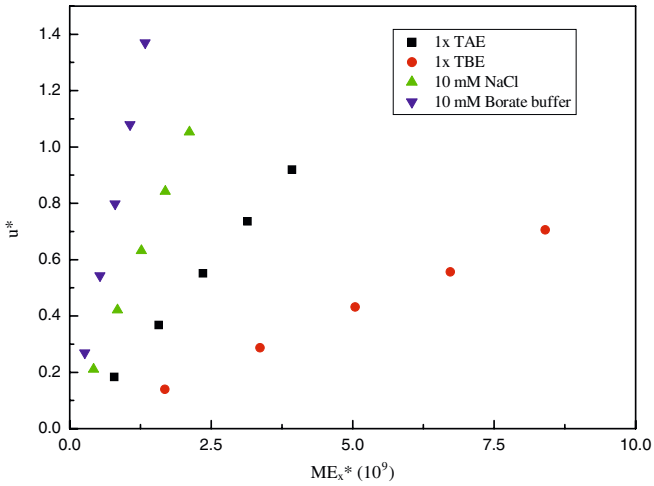


**Fig. 10** Dimensionless average velocity vs dimensionless group $ME_x^*$

and $e$ the charge of a negative ion. $\overline{u}_m$ was defined in Eq. (3) and, in fact, can be obtained from the MPIV measurements. The results were replotted against $E_x$ for four buffers as shown in Fig. 8 where nonlinear increases are again noted due to Joule heating. Like previously stated, this is because Joule heating gives rise to significant buffer temperature increases. Joule heating due to electric current took place uniformly over the entire volume of the present flow, and its value can be estimated, and found to be dependent on $D_h$, and applied electric strength. Based on the values given in Table 1, the Joule heating of the present study is dominating when the externally applied electric field is bigger than 15 kV/m. Simultaneously, this modification counts electrophoretic mobility increases in Fig. 8 while a constant mobility was assumed in Fig. 7a. Figure 9 summarizes the present measurement results with/without Joule heating and results calculated with modifications. It can clearly be noted that the measurements with Joule heating are quite in accordance with those from modifications through Eq. (3). Also included in Fig. 9 are results from Sinton and Li [11]. The discrepancy was expected due to a higher pH value in 1× TAE of Sinton and Li [11], which would result in an immediate effect on the magnitude of the EOF.

**Table 2** Uncertainties analysis for relevant variables and parameters

| | Parameters/Variables | System error (%) | Random error (%) |
|---|---|---|---|
| Geometric parameters | $L$ (μm) | 0.09 | 0.02 |
| | $H$ (μm) | 0.13 | 0.05 |
| | $W$ (μm) | 0.15 | 0.04 |
| TAE | Concentration | 2.17 | 2.33 |
| | Particle velocity | 0.17 | 2.08 |
| | Total velocity | 0.40 | 2.19 |
| | Osmotic velocity | 0.57 | 4.27 |
| | Mobility | 2.08 | 4.72 |
| TBE | Concentration | 2.03 | 2.52 |
| | Particle velocity | 0.18 | 1.15 |
| | Total velocity | 0.26 | 2.75 |
| | Osmotic velocity | 0.44 | 3.90 |
| | Mobility | 2.05 | 4.39 |
| NaCl | Concentration | 3.99 | 4.33 |
| | Particle velocity | 0.17 | 3.49 |
| | Total velocity | 0.65 | 1.69 |
| | Osmotic velocity | 0.82 | 5.18 |
| | Mobility | 2.16 | 5.55 |
| Borate buffer | Concentration | 3.80 | 4.17 |
| | Particle velocity | 0.18 | 1.57 |
| | Total velocity | 0.39 | 2.88 |
| | Osmotic velocity | 0.57 | 4.45 |
| | Mobility | 2.08 | 4.88 |

Figure 10 shows that the dimensionless velocity $u^*$ was plotted against dimensionless $ME_x^*$. Again, the data presented are more or less linear and extend through origin. Four distinct lines are shown, and each stands for a definite Debye number (DN), defined as $D_h/\lambda$, with values of 93,300, 13,9800, 65,800, and 52,400, respectively, and different $\varsigma^*$, indicated in Fig. 11a, for 1× TAE, 1× TBE, 10 mM NaCl, and 10 mM borate buffers. Actually, $\varsigma^*$ is an intrinsic property of the channel material and electrolyte ions. The highest $u^*$ was found at the smallest DN=52,400, while the lowest $u^*$ was found at the largest DN=139,800 as one would expect. Obviously, the present EOF was strongly dependent on DN. Each corresponding Debye length is listed in Table 1. As one can see, 1× TBE has the smallest Debye length (~1.43 nm) and the largest DN due to a strong ion concentration in 1× TBE buffer as stated previously. Furthermore, the present EOF is also influenced by an external electrical field strength $E_x$ as discussed earlier. Similarly, the ionic strength also influences zeta potential and results in a lower zeta potential as the ionic strength is increased. A functional relationship among $u^*$ with $\varsigma^*$, DN, and $ME_x^*$ is developed and plotted in Fig. 11a,b. The influences of $\varsigma^*$, DN, and $ME_x^*$ on $u^*$ can clearly be examined. $u^*$ is directly proportional to $\varsigma^*$ and $ME_x^*$ with the exponents of 0.739 and 0.9996, respectively, and inversely proportional to DN with a relatively high exponential power of 2.132. Based on these two plots, $u^*$ can be correlated in the following form:

$$u^* = 5.46\,\varsigma^{*0.739} DN^{-2.132} ME_x^{*0.9996} . \quad (4)$$

It can be seen that the $u^*$ dependency on $\varsigma^*$ and $ME_x^*$ is almost equal. However, DN has the strongest influence on $u^*$ among these three parameters. Overall, these three parameters would definitely influence $u^*$ significantly in the present EOF. Figure 12 shows that the discrepancy

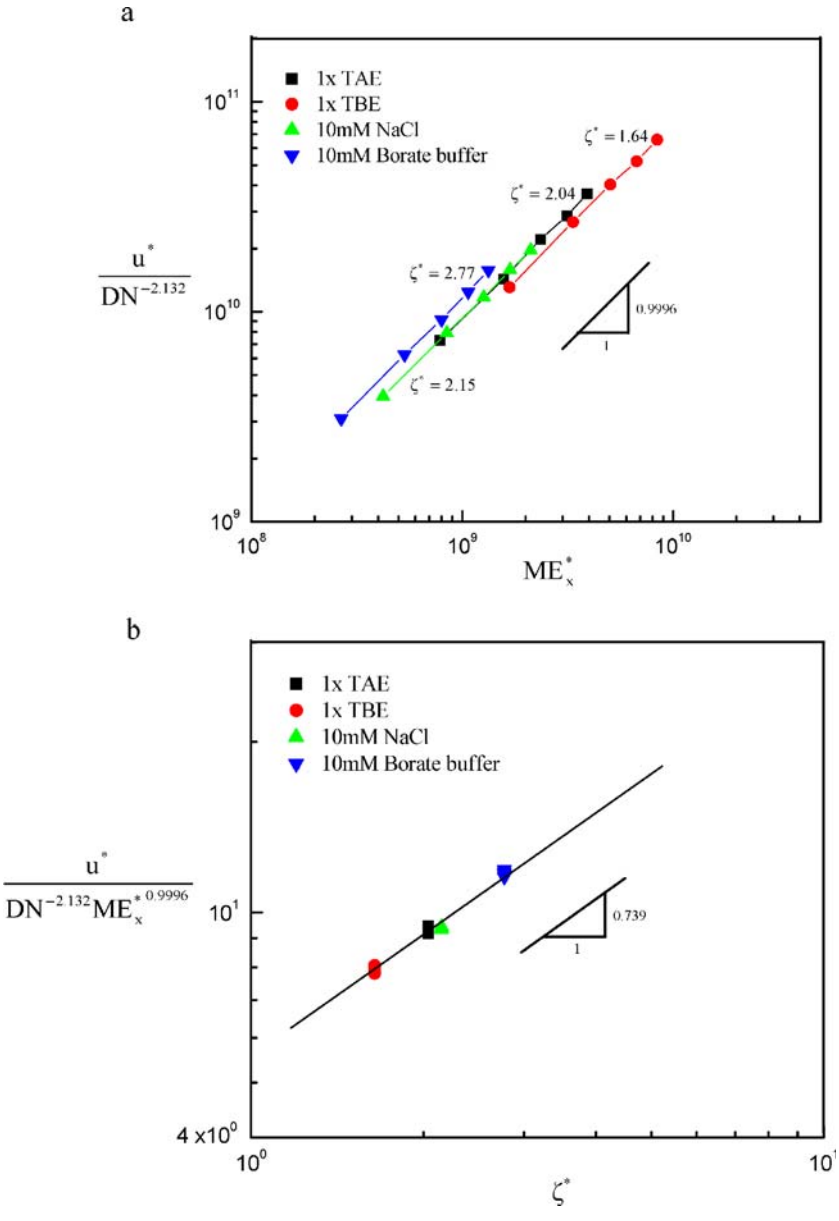


**Fig. 11** The functional relationship of $u^*$ on $\zeta^*$, DN, and $ME_x^*$

**Table 3** Electrophoretic mobility, electroosmotic mobility, and zeta potential comparison

| | 1× TAE | 1× TBE | 10 mM NaCl | 10 mM Borate buffer |
|---|---|---|---|---|
| Electrophoretic mobility ($10^{-8}$ $m^2$/V s) | 4.71 | 4.36 | 4.85 | 4.37 |
| Devasenathipathy and Santiago [3] | | | | 4.29 |
| Electroosmotic mobility ($10^{-8}$ $m^2$/V s) | 3.68 | 2.84 | 4.21 | 5.43 |
| Sinton et al. [12] | 4.90 | 3.10 | | |
| Devasenathipathy and Santiago [3] | | | | 5.17 |
| Zeta potential (mV), $\zeta$ | −52.38 | −42.24 | −55.32 | −71.21 |
| Sinton et al. [12] | −63.00 | −40.00 | | |

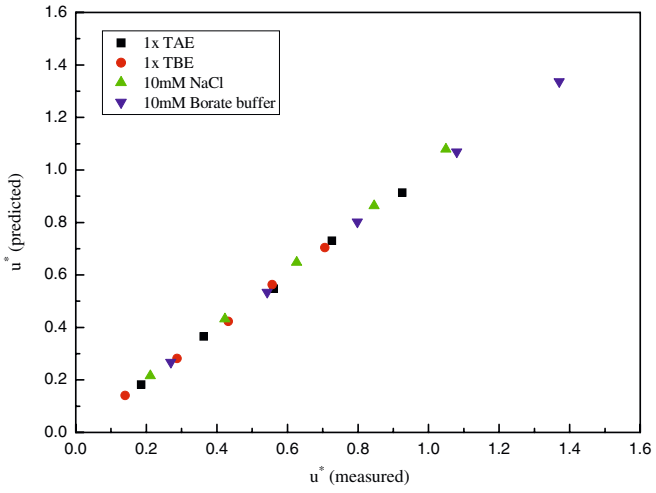


**Fig. 12** $u^*$ (measured) vs $u^*$ (predicted)

between the prediction using Eq. (4) and the measured $u^*$ is within ±1% accuracy for about 99% experimental data.

## Conclusions

The velocity distribution as well as 2D velocity vector fields through a direct method of EOF in a square microchannel of a hydraulic diameter of 200 μm for four different buffers has been investigated experimentally in this study. Parametric examination of ionic strength and external applied electric strength in terms of a dimensionless parameter $ME_x^*$ dimensionless zeta potential $\varsigma^*$ and Debye number ($=D_h/\lambda$) incorporated with MPIV measurements was systematically conducted. The results demonstrate the significance of different buffers' effect due to different Debye length (i.e., different DN also). Increases in $E_x^*$ would increase the EOF velocity; however, there seems little impact on it due to an increase in $M$. Most present results in velocity distributions with/without Joule heating are in good agreement with those of previous studies in both trends and magnitude. With these conditions, constant electroosmotic mobility values of $3.68\times10^{-8}$, $2.84\times10^{-8}$, $4.21\times10^{-8}$, and $5.43\times10^{-8}$ $m^2/V$ s for 1× TAE, 1× TBE, 10 mM NaCl, and 10 mM borate buffers, respectively, were obtained. A functional relationship was finally developed in terms of the relevant parameters.

**Acknowledgement** This work was supported by the National Science Council, Taiwan, ROC under contract number NSC 94-2212-E-110-025.

## References

1. Arulanandam S, Li D (2000) Liquid transport in rectangular microchannels by electroosmotic pumping. Colloids Surf A Physicochem Eng Asp 161: 89–102
2. Cummings EB (1999) PIV measurement of electroosmotic and pressure driven flow components in microfluidic systems. J Microelectromech Syst 1:377–381
3. Devasenathipathy S, Santiago JG (2002) Particle tracking techniques for electrokinetic microchannel flows. Anal Chem 74:3704–3713
4. Duffy DC, McDonald JC, Schueller OJA, Whitesides GM (1998) Rapid prototyping of microfluidic systems in poly(dimethyl siloxane). Anal Chem 70:4974–4984
5. Dutta P, Kim MJ, Kihm KD, Beskok A (2001) "Electroosmotic flow in a grooved micro-channel configuration: a comparative study of μPIV measurements and numerical simulations," Proceedings of 2001 ASME international mechanical engineering congress and exposition, New York, NY, USA, 11–16 November 2001
6. Hsieh S-S, Kuo J-K, Hwang C-F, Tsai H-H (2004) A novel design and microfabrication for a micro PEMFC. Microsyst Technol 10:121–126
7. Hunter RJ (1981) Zeta potential in colloid science: principles and applications. Academic, New York
8. Kim MJ, Kim HJ, Kihm KD (2001) "Micro-scale PIV for electroosmotic flow measurement." In: Proceedings of PSFVIP-3, Maui, Hawaii, USA, 18–21 March 2001
9. Maynes D, Webb BW (2003) Fully developed thermal transport in combined pressure and electro-osmotically driven flow in microchannels. J Heat Transfer 125:889–895
10. Meinhart CD, Wereley ST, Santiago JG (1999) PIV measurements of a microchannel flow. Exp Fluids 27:414–419
11. Sinton D, Li D (2003) Electroosmotic velocity profiles in microchannels. Colloids Surf A Physicochem Eng Asp 222:273–283
12. Sinton D, Escobedo-Canseco C, Ren L, Li D (2002) Direct and indirect electroosmotic flow velocity measurements in microchannels. J Colloid Interface Sci 254:184–189
13. Yang J, Kwok DY (2002) A new method to determine zeta potential and slip coefficient simultaneously. J Phys Chem B 106:12851–12855